Separation Science and Technology
Publication details, including instructions for authors and subscription information:
http://www.informaworld.com/smpp/title~content=t713708471

CFD Simulation of the Separation Zone of an Annular Centrifugal Contactor

Kent E. Wardle[a]; Todd R. Allen[a]; Ross Swaney[b]
[a] University of Wisconsin-Madison, Department of Engineering Physics, Madison, WI, USA [b] University of Wisconsin-Madison, Department of Chemical and Biological Engineering, Madison, WI, USA

Online publication date: 22 June 2010

To cite this Article Wardle, Kent E. , Allen, Todd R. and Swaney, Ross(2009) 'CFD Simulation of the Separation Zone of an Annular Centrifugal Contactor', Separation Science and Technology, 44: 3, 517 — 542
To link to this Article: DOI: 10.1080/01496390802634398
URL: http://dx.doi.org/10.1080/01496390802634398

Separation Science and Technology, 44: 517–542, 2009

ISSN: 0149-6395 print/1520-5754 online
DOI: 10.1080/01496390802634398

Taylor & Francis
Taylor & Francis Group

CFD Simulation of the Separation Zone of an Annular Centrifugal Contactor

Kent E. Wardle,[1] Todd R. Allen,[1] and Ross Swaney[2]
[1]University of Wisconsin–Madison, Department of Engineering Physics, Madison, WI, USA
[2]University of Wisconsin–Madison, Department of Chemical and Biological Engineering, Madison, WI, USA

Abstract: This paper presents computational fluid dynamics (CFD) simulations of the flow inside the rotor of an annular centrifugal contactor. The model geometry was based on the rotor of a commercially available contactor unit with a closed upper weir. Simulations were performed at various flow rates and it was found that the narrow flow area above the upper weir seals with water at high flow rates resulting in the formation of a siphon. A method for predicting the zero-point flow rate from CFD was also developed and simulations were performed which demonstrate a zero-point elevation due to this siphon.

Keywords: Computational fluid dynamics (CFD), solvent extraction, centrifugal contactors, liquid-liquid separation, reprocessing

INTRODUCTION

Advanced solvent extraction processes have been developed for separation and recycle of usable components in used nuclear reactor fuel (1). A central piece of equipment for such processes is the annular centrifugal contactor—a compact device that enables high process throughputs as compared to typical liquid-liquid extraction equipment due to its use of centrifugal separation of the liquid phases inside a hollow rotor. This rotor also provides the driving force for mixing in an annular region

Received 2 July 2008; accepted 27 October 2008.
Address correspondence to Kent E. Wardle, Argonne National Laboratory, 9700 S. Cass Avenue, Argonne, IL 60439, USA. E-mail: kwardle@anl.gov

outside the rotor. Figure 1 shows a sketch of a typical annular centrifugal contactor.

The mechanically simple design of this equipment (one moving part—the rotor) facilitates the remote operation and maintenance required for processing used nuclear fuel—the original focus for contactor development (2). Beyond used fuel processing, such contactors can enable process intensification in a variety of other fields where liquid–liquid extraction is used. The research presented here of simulations of the flow in the contactor separation zone (i.e. inside the rotor) is part of a broader effort to improve the understanding of the flow within all areas of the centrifugal contactor through the application of computational fluid dynamics (CFD) coupled with a variety of experimental observations (3).

Heretofore CFD modeling techniques have not been applied to rotor design. However, a useful analytical approach has been demonstrated for

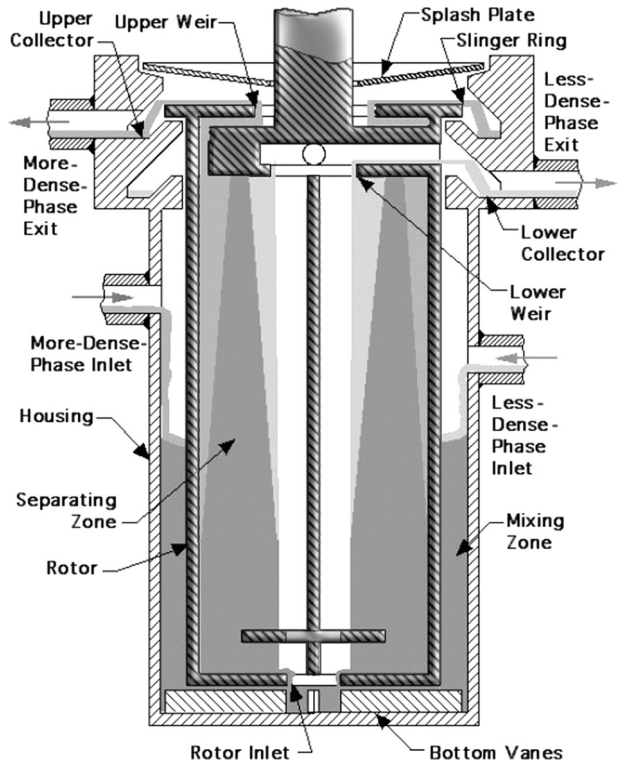

Figure 1. Sketch of an annular centrifugal contactor. Figure taken from Leonard et al. 2002.

determining the proper dimensions of the weirs based primarily on experimental correlations and hydrostatic balance arguments (4). While this method has been generally quite successful for rotor sizing of contactors with an open upper weir (and the obsolete air-controlled upper weir), some experiments with 'closed' upper weir systems have produced behavior which cannot fully be explained by the existing theoretical models. One such unexplained behavior is the elevated throughput that has been observed for large upper weir sizes in these units (5). This same behavior has also been observed in larger units of this design (6). One of the main goals of this overall research effort is to demonstrate CFD as a useful tool not only to aid in the design of future contactor units, but also to provide a valuable method for critical evaluation of current designs and support deployment of these contactors. As with separate models of the contactor's annular mixing zone (7,8), the basis for the separation zone geometry simulated here is the Costner Industry Nevada Corporation's (CINC) V-2 contactor unit; this product line is currently the only commercially available annular-type centrifugal contactor in the United States. Units of this design were used for various research and development efforts related to the Caustic Side Solvent Extraction (CSSX) process for cesium extraction (5,9–11) and will presently be used in actual plant implementation of this process; analysis of the flow in this specific design is therefore particularly relevant.

To the authors' knowledge there is only one other published study which attempts to apply CFD to the separation zone of an annular centrifugal contactor. That study by Padial-Collins et al. of Los Alamos National Laboratory (12) was primarily a code capability demonstration looking at the separation of the liquid mixture; their simulations employed a substantially simplified rotor geometry and did not consider the flow of air or the liquid/air interface within the rotor. Better understanding of the flow within the rotor and specifically the flow over the weirs requires full simulation of the complex rotor and weir geometries and analysis of the liquid free surface flow as done in the work presented here. Further, such hydraulic simulations can calculate important flow quantities which characterize the rotor and weirs such as the zero-point flow rate (4,5).

While the geometry of the mixing zone is quite amenable to external observation (for example see Wardle et al. 2008 (7,13)), similar detailed experimental observations such as velocity measurements for the flow within the rotor were not possible. Therefore, the work presented here relies primarily on the results of computational analyses with the support of certain experimental observations made within the context of this current work as well as by others.

Flow Within the Rotor

Unlike the mixing zone, there has been no direct observation of the flow within the contactor rotor. Consequently, the simulations presented here have utility simply as a tool for visualizing the flow in this region. Beyond this simple qualitative application, these simulations can provide a means for improving understanding of the flow in this region.

The role of the centrifugal contactor for use in liquid–liquid extraction is to thoroughly and efficiently mix the two process fluids and then in an equally thorough and efficient manner separate them completely. The separation occurs as the dispersion of the two liquid phases enters the hollow rotor through the inlet at the bottom. The centrifugal action of the spinning rotor forces the fluids outward and the phases separate due to their density differences as they steadily flow upward. The flow in the rotor is roughly analogous to that in a two-phase gravity settling trough as shown in Fig. 2. In the case of the centrifugal contactor, however, the orientation is vertical and at typical operating speeds (around 3600 RPM for a 5 cm rotor) the outward force at the outer wall is caused by an acceleration a few hundred times that of gravity. Thus, the orientation relative to gravity becomes negligible at high speeds and the flow (relative to the axis of the rotor) appears similar in principle to the settling trough. Of course, just within the rotor inlet as well as just above the weirs, the tangential velocity of the fluid relative to the rotor rotation is significant and the simple comparison to the horizontal trough breaks down.

For liquid–liquid separation, as the flow rate is increased the width of the dispersion band (the region of unseparated fluid mixture) at the top of the active separating height (the underside of the light phase weir) increases. Depending on the organic-to-aqueous flow ratio (O/A) and the weir radii, there is a maximum flow rate at which the width of the dispersion band is equal to the radial difference between the light phase weir and the heavy phase underflow slot. Increasing the flow rate of either

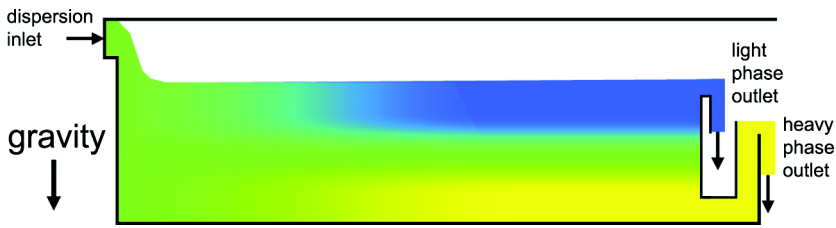

Figure 2. Sketch of a horizontal two-phase gravity settling trough (online version contains color reproduction).

phase results in phase carryover into the other stream. Theoretical models developed at the Argonne National Laboratory have employed hydrostatic balance techniques coupled with experimental correlation to predict this behavior and aid in selection of the optimum weir sizes for a given throughput and O/A ratio (or visa-versa) (4,5).

For single liquid phase flow in the contactor rotor, the focus of this study, an important characterizing parameter is the flow rate at which the separation zone becomes filled—that is, the point at which the single-phase flow rate entering the rotor is such that the liquid volume maintained in the rotor increases to the point where flow begins to come out the light phase exit port. This is referred to as the zero-point flow rate. The Argonne model is capable of accurately predicting this point if the pressure above the upper weir is known. For an open upper weir such as is shown in the general contactor sketch in Fig. 1, the pressure is equal to the atmospheric pressure (the splash plate is not air tight on the rotor shaft). Similarly for an air-controlled upper weir the air pressure is a known specified value (4). Along with analyzing the general single-liquid flow characteristic in the separation zone, another purpose of this current modeling effort is to examine the behavior of the closed upper weir of the CINC rotor.*

Experimental Methods

The experimental setup that was used for the selected measurements reported here has been described in detail elsewhere (3,7,13). It consisted of a 5 cm (rotor diameter) centrifugal contactor manufactured by Costner Industry Nevada Corporation (CINC). Experimental measurements of the zero-point flow rate were made for three different upper weir radii (1.08 cm, 1.15 cm, and 1.175 cm) both with the standard ''closed'' upper weir cap as well as with a modified ''vented'' cap described below. For these measurements a single pump was used with equal flow distribution to the two tangential inlet ports.

COMPUTATIONAL METHODS

Computational modeling of the 3D, two-phase (air/water) flow within the rotor was done using the commercial CFD package Fluent 6.3. As

*The purpose of this upper weir cap which effectively closes the upper weir is to hold the removable weir plate in place. For a permanent upper weir plate, the weir cap should be unnecessary.

with the simulations of the flow in the mixing zone reported elsewhere (7,8), the Volume of Fluid (VOF) method with piecewise linear interface construction (PLIC) was used to track the volume fraction and simulate the physics of the air/water free surface. Surface tension was included using the Continuum Surface Force method (14) with a value of 73 dynes/cm (air/water interfacial tension) and the water contact angle on all surfaces was set at 75° to simulate the contact of water on steel in air. Additionally, it was assumed that the flow in this region of the contactor is laminar. All simulations were time-dependent using Fluent's non-iterative time advancement (NITA) solver (15) and most were performed in parallel using 10–20 processors. Some were done using a local Linux cluster and others were executed on the Tungsten Xeon Linux Cluster at the National Center for Supercomputing Applications (NCSA).

Geometry and Mesh

The geometry used for the separation zone model was based on the rotor of the commercially available CINC V-2 contactor (see Fig. 3 (16)). As no official drawings of this contactor rotor were available, the various dimensions were directly measured by micrometer and a computer model was thus directly constructed from the physical dimensions of the rotor. In order to minimize the computational cost by taking advantage of symmetry, only a one-quarter section was modeled with 90° rotationally periodic boundary conditions. Figure 4 shows several views of the model rotor geometry. As this geometry is quite complex, a complete list of

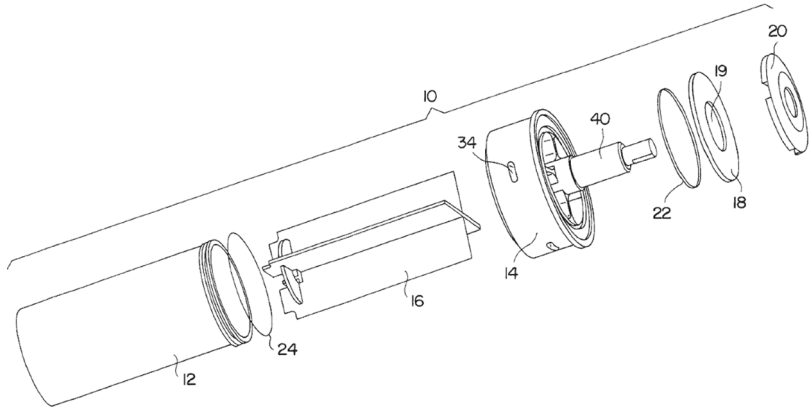

Figure 3. Diagram of an exploded view of the rotor of a CINC V-2 centrifugal contactor. Figure taken from Sheldon et al. 2002 patent.

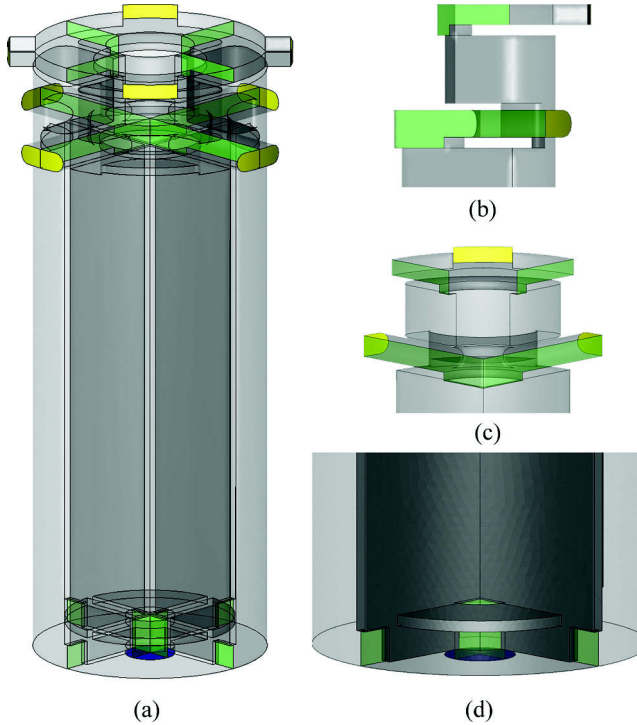

Figure 4. Separation zone model. Pressure outlets are colored yellow, the mass flow inlet blue, and all periodic boundaries green. (a) Full model including periodic images of the modeled quadrant. (b) Side view of upper section of model quadrant showing 'tiered' heavy phase underflow. (c) Angled view of upper section of the model quadrant showing weirs. (d) Close view of bottom section (with periodic images) showing inlet, diverter disk, and divider vanes with a notched flow passage at the bottom outer edge (online version contains color reproduction).

dimensions will not be included here; several important dimensions of the model rotor geometry are given in Table 1.

Two different upper weir dimensions are listed in the table; the larger 1.15 cm weir radius was used for all of the simulations. The zero-point simulations described later were also repeated using a smaller, 1.08 cm radius for additional comparison with the experimental measurements of the zero-point. The separation height h_{sep} is the height from the interior bottom of the rotor to the underside of the light phase weir. The heavy phase underflow height listed in Table 1 is the vertical distance between the underside of the lower weir and the underside of the upper weir plate.

Table 1. Selected dimensions of the contactor separation zone model

Parameter	Symbol	Value, cm
Inner Radius	r_{in}	2.38
Separation Height	h_{sep}	10.60
Heavy Phase Underflow Height	h_{aq}	1.66
Lower Weir Radius	$r_{w,\ lower}$	1.037
Light Phase Exit Radius	r_{light}	3.15
Upper Weir Radius	$r_{w,\ upper}$	1.15 (0.45'')
		1.08 (0.425'') (zero-pt only)
Heavy Phase Exit Radius	r_{heavy}	2.90
Flow Height Above Upper Weir	h_{upper}	0.30

The upper weir plate (labeled 18 in Fig. 3) is held in place by a weir cap (item 20)[†] that forms the upper flow section and the four rectangular heavy phase outlet channels shown in the model (see Fig. 4(a)). The height of the flow area above the weir h_{upper} is only 3 mm. As will be shown with the results of these simulations and experiments, this restricted flow area has an impact on the high flow rate operation of the rotor. Notice also that the heavy phase outlet and light phase outlet are staggered at 45° relative to one another. While care was taken to include each detail of the actual rotor geometry, one subtle but perhaps important difference between the real rotor and the model rotor is that the weirs in the model both have a perfectly sharp edge. This is a good representation of the actual features of the experimental apparatus when it comes to the light phase weir; however, the heavy phase weir in the CINC V-2 unit has a slightly beveled edge. For certain quantities of interest such as the zero-point flow rate, this difference may impact direct quantitative comparison with experiment.

The mesh was created using Gambit 2.4 and consisted of all unstructured, tetrahedral cells with nodes clustered near the inlet and bottom surfaces as well as in the upper region of the rotor around the weirs and the surface of the upper weir to achieve better resolution of the gas–liquid interface at these critical sections. The necessity of

[†]The weir cap is machined such that it fits comfortably around the rotor shaft although there seems to be some variability between units in the tightness of this cap around the rotor shaft. For the experimental measurements of the zero-point reported here a layer of seal tape on the rotor shaft was used to ensure air-tightness and consistency of measurements and provide the best comparison with the model geometry.

transient simulations for the VOF method used here made it such that the overall mesh density was primarily limited by computational cost and a full grid resolution study was not feasible. Two different levels of meshing were used for the simulations presented here. For simulations of the general flow for which a detailed solution at a given flow rate was desired, a finer mesh was applied. For simulations aimed at determining the zero-point flow rate, which required simulations over relatively long times for varying inlet flow rates, a more coarse mesh was used. As will be described later, simulations (and experiments) with a modified "vented" upper weir cap were also performed. The number of computational cells for each of the various models and meshes used are listed in Table 2.

Model Setup

The inlet to the separation zone was treated as a spatially and temporally constant mass flow rate boundary. While it was possible to apply a mass flow rate profile across this boundary, even taking it directly from the average profile at the exit of the mixing zone model (7) for the case where the total flow rate simulated was the same, it was found that this did not have a noticeable effect on the predicted flow field and therefore a constant value boundary condition was applied. The inlet boundary also did not have a specified tangential velocity. The inlet to the separation zone model is flush with the outer bottom surface of the rotor and therefore this is an acceptable boundary condition since there is little rotation of the flow there and it is only once the flow enters the rotor inlet that it begins to be significantly re-accelerated. Separate simulations looking at the general flow in the rotor were performed at two different inlet flow rate settings: 600 ml/min and 1600 ml/min. For the simulations used to predict the zero-point flow rate, the inlet flow rate was not fixed, but was adjusted using a function coupling it to the overall mass balance and the position of the air/water interface relative to the lower weir. This

Table 2. Number of computational cells for the various separation zone meshes

Weir cap type	Upper weir radius, cm	N cells	Simulation type
Standard	1.15	311 K	General Flow
Standard	1.15	146 K	Zero-point
Vented	1.15	178 K	Zero-point
Standard	1.08	159 K	Zero-point
Vented	1.08	165 K	Zero-point

Table 3. Zero-point flow rate values predicted from CFD simulation. For general comparison of the trends, values observed experimentally for the same contactor unit are also shown

Weir cap	Aq. weir radius, cm	Zero-point flow rates, ml/min		
		Simulation	Current experiment	Leonard et al. (5)
Standard	1.08	287	431	467
Vented	1.08	290	375	n/a
Standard	1.15	2230	1571	1592
Vented	1.15	1451	1343	n/a
Standard	1.175	–	2408	2753
Vented	1.175	–	1907	n/a

was done using a piece of add-on code referred to as a User-Defined Function (UDF) in Fluent and is discussed more later.

Each of the phase outlets (light phase and heavy phase) was specified as a pressure outlet with the boundary pressure set equal to atmospheric pressure. The backflow condition was specified with a liquid volume fraction equal to zero—that is, if there was reverse flow (which indeed there was at the light phase exit) it would be air, consistent with the real case. A rotational speed of 3600 RPM was applied to the entire fluid domain and the velocity field was solved for within this single rotating frame of reference.

These simulations were time-dependent and employed a variable time step according to the Courant flow number Cr which is defined as:

$$Cr = \frac{\Delta t}{\Delta x/u} \approx 0.25 \tag{1}$$

where u is the local air/liquid interface velocity and Δx is the local grid spacing. The typical time step Δt for the finer mesh simulations was approximately 16 μs while that for the zero-point simulation meshes was 20–30 μs. Typical simulation times were about 70 hours per 1 s of flow for the general flow simulations (on 20 processors) and 40–50 hours per 1 s for the smaller zero-point simulations (on 10 processors). Because of the relatively long flow times (several seconds at least) that were required for the zero-point flow rate simulations, the global Cr number that determined the overall time step was increased as much as possible while still maintaining adequate convergence and good stability at each time step; for these simulations, the global Cr number was as much as 5.0. Even so, the local Cr number limit of 0.25 necessary for the VOF

model is still maintained within Fluent by applying sub-time stepping for the volume fraction calculation (15). The initial simulation of the separation zone was started from the rest with a fixed liquid height and all subsequent simulations were initiated with a patched-in velocity field for the flow already in motion to avoid this start-up time. The liquid volume in the model was allowed to equilibrate before any steady-state flow observations were made. The characteristic equilibration time was much slower for the separation zone than for the mixing zone. Whereas it was observed that the flow in the mixing zone achieved liquid hold-up volume equilibration following a moderate change in flow conditions within about 1 s of flow time (3), equilibration for the separation zone took several seconds of flow (~3–5 s) for similar changes. This difference is simply related to the large difference in the liquid volumes maintained in each region. The nominal liquid volume in the separation zone is approximately 160 ml. This is several times that of the mixing zone (see Wardle et al. 2008 (8)) and translates into a mean fluid residence time within the rotor several times larger than that in the annular region. The difference in the overall response time scales of the two regions has implications for understanding how process upsets effect the performance of the equipment.

RESULTS AND DISCUSSION

General Flow

Simulations of the flow in the separation zone using the more refined mesh were performed at two different flow rates, the standard 600 ml/min and a much higher 1600 ml/min. Both of these were for the larger (1.15 cm) upper weir. Note that 1600 ml/min is very near the experimentally observed zero-point flow rate of 1592 ml/min which was measured previously by others for flow in this very same contactor unit (5). The general flow behavior for these two flow rate settings will be discussed here.

Air Core

Figure 5 shows a cross-section view of the flow of water (red) and air (blue) in the separation zone of the contactor for the two inlet flow rate settings. The more diffuse appearance of the air/water interface in the central portion of the separating region above the diverter disk and below the lower weir is simply an artifact of the larger computational cells used

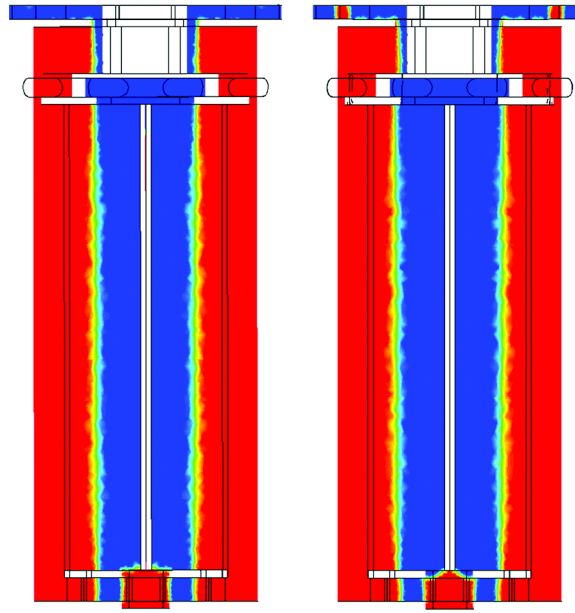

Figure 5. Cross-section plots of the water volume fraction distribution in the separation zone at 600 ml/min (a) and 1600 ml/min (b). The vertical cross-section shown here bisects the regions between rotor vanes (online version contains color reproduction).

in this region. From this cross-sectional view, there are only subtle differences between the two flow rate settings. As will be described in more detail in the following two sections, these differences occur primarily near the inlet and above the upper weir. The distinctive feature of the flow in the main separation region of the rotor is the essentially vertical air/water free surface. As both simulations were for flow at the same rotor speed (3600 RPM) it is not surprising that the general position and shape of the free surface is consistent between the two. It was observed for some initial scoping simulations of the separation zone that the free-surface becomes more parabolic at lower rotor speeds ($\sim$1500 RPM).

It was also observed that there was a radially recirculating flow of air in the organic exit channels as these were empty of water and open to the atmosphere for both settings. This allowed for a balance in the volume of air in the rotor as the volume of water increased to the equilibrium level from the initial starting volume. For the higher flow rate setting there was not as yet any flow out of the light phase exit port as would be expected if

the zero-point had been exceeded. In fact, as will be discussed later the features of the flow above the upper weir lead to a significant elevation in the predicted zero-point flow rate.

Flow Near Inlet

As shown in Fig. 4(d), there are vanes within the rotor that divide the interior of the rotor into four separate regions. For most of the height, these vanes seem to have little effect (i.e. there is very little azimuthal variation in the flow). However, they are very important near the inlet as they force the fluid entering the rotor to quickly accelerate up to the speed of the rotor. In practical terms, the separate regions also help to maintain balance of the spinning, fluid-filled rotor. Near the inlet, these vanes actually do not extend all the way to the axis of the rotor and there is an open section below the diverter disk (which also has a hole in it). The flow simulations predict that near the inlet there is a stable column of liquid that is maintained below the diverter disk in this empty region near the axis where the vanes do not extend.

The sweeping of the rotor vanes pumps the fluid from the edge of this water column radially outward into the rotor. This behavior can be observed in Fig. 6 which shows the flow of water on the rotor vanes (as well as a cross-section of the inlet water column). This image is at 45° relative to the one shown in Fig. 5 in order to show the flow on the surface of the vanes rather than between them as in that previous figure. At the lower flow rate (Fig. 6(a)), it appears that the flow is by droplets or very thin "filmlets" on the backside vane. There is also some flow traveling up through the hole in the diverter disk and then being propelled outward. For the higher flow rate setting (Fig. 6(b)), there is a continuous layer of water on the backside vane. Notice that the force of this water layer as it flows radially outward also results in the entrainment of air which collects within the small channels that pass through the

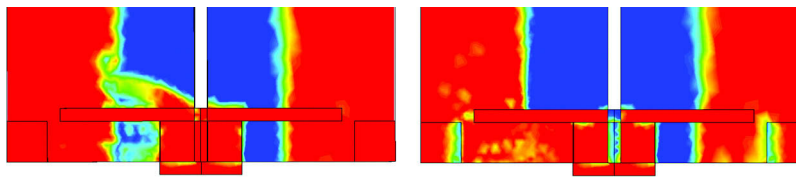

Figure 6. Cross-section of water volume fractions near the inlet and on the rotor vane walls for flow rates of 600 ml/min (a) and 1600 ml/min (b) (online version contains color reproduction).

vanes at the outer bottom corner to allow redistribution of fluid between the regions.

These same effects can be further observed in the differences in the velocity field on the bottom surface of the interior of the rotor as shown in Fig. 7. In this figure the velocity field (for both phases) relative to the

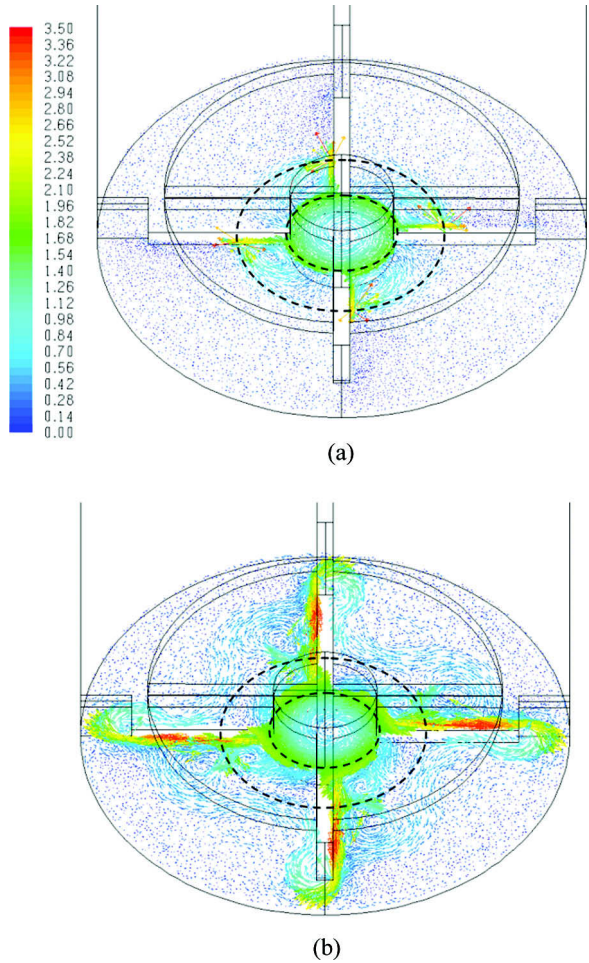

Figure 7. Velocity vectors showing flow relative to the rotor rotation on the bottom interior surface of the rotor for flow rates of 600 ml/min (a) and 1600 ml/min (b). The dashed circles denote the general locations of the inlet water column (inner circle) and the outer free surface at the inner edge of the main fluid region (outer circle) [see Figure 5]. An outline of the lower portion of the rotor geometry is also visible.

rotor rotation is shown; thus, the magnitude of the tangential velocity is highest near the inlet where the water entering the rotor has a rotational speed less than that of the rotor but is being accelerated. Conversely, the magnitude of the difference between the rotor velocity and the fluid velocity is small near the outer wall and therefore the vectors are small. From Fig. 7(a) it is clear that there is little radial transference of momentum across the air gap between the inlet water column and the outer main fluid volume for the lower flow rate setting. On the other hand, there is significant radial momentum transported within the continuous water film propelled outward by the vane for the 1600 ml/min case (Fig. 7(b)). For this case, there is flow that extends all the way to the inter-vane channel and then sweeps back down the rotor vane towards the free surface at the edge of the air core. Recall that it was assumed that the flow is laminar in the separation zone. While this is likely an adequate approximation, in reality there is certainly decaying turbulence and perhaps even some turbulence generation near the bottom of the separation zone where large velocity gradients exist while the fluid is being accelerated (such as depicted in Fig. 7(b)).

Flow Above Heavy Phase (Upper) Weir

Unlike most contactors, the CINC centrifugal contactor has a removable upper weir that is held in place by a cap that imposes a boundary effectively forming a narrow flow area above the upper weir. From the simulations of the two different inlet flow rates, this feature was found to have a pronounced effect on the overall flow behavior.

The flow over the upper weir at 600 ml/min had the general characteristics expected for flow over a completely open upper weir, consisting primarily of droplet/rivulet flow from the inner weir edge outward along the surface of the weir. An instantaneous snapshot of the flow above the upper weir as predicted by simulation is shown in Fig. 8(a) and to give a better view of the flow paths of the individual droplets, a time average of the water volume fractions is shown in Fig. 8(b). The flow over the weir is primarily as discrete droplets which curve outward with decreasing tangential velocity relative to the rotor speed. Note that droplets which impinge on the outer surface of the weir cap tend to "climb" up the wall and link up with droplets below them. The droplets then accumulate as a film on the backside of the outlet channel where they exit the rotor model and are spun out into the collector rings.

A dramatic difference for flow in the same region at the higher flow rate (1600 ml/min) can be seen in Fig. 9. Only an instantaneous snapshot is shown as there was very little time variation of the flow for

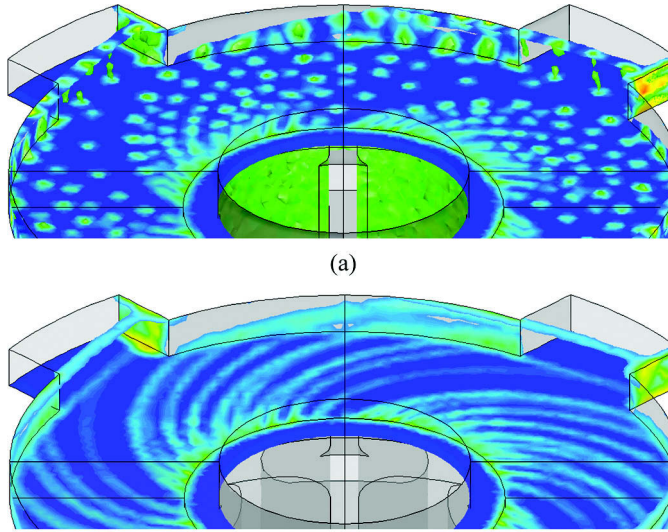

Figure 8. Plot of instantaneous (a) and mean (b) water volume fractions on the top surface of the upper weir and water contacted areas of the upper weir cap at 600 ml/min and 3600 RPM. Rotation is in the counter-clockwise direction. Periodic images of the modeled quarter-section are shown for continuity (online version contains color reproduction).

this case.[‡] The simulation shows that the air space above the upper weir no longer has open communication with the outside (atmospheric) pressure and has been completely sealed by a ring of water. The radial thickness of this water ring is ~2 mm. Previous hydrostatic balance-based models of the rotor (4,5) assume that the pressure above the upper weir is equal to atmospheric pressure. For the case shown in Fig. 9 it is obvious that such an assumption may be invalid for the current configuration. The pressure above the upper weir as predicted by this simulation is approximately −1900 Pa for this flow rate as compared to only −30 Pa for the 600 ml/min case. The behavior of the flow in this

[‡]Because the free surface position does not vary significantly in the rotor for most cases, originally steady-state calculations were attempted. These were found to be unsolvable likely due to the interface discontinuities above the upper weir and therefore were abandoned. It may be possible to obtain a converged time-invariant solution for high flow rates such shown in Fig. 9 although this was not attempted.

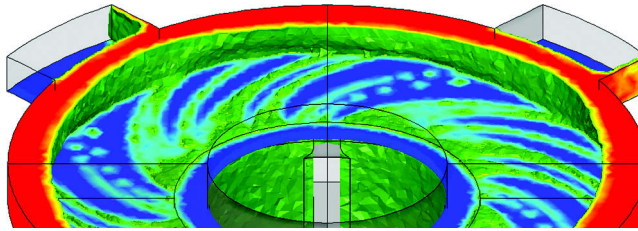

Figure 9. Plot of the instantaneous water volume fractions above the upper weir at 1600 ml/min (3600 RPM) (online version contains color reproduction).

"water-sealed" case is somewhat analogous to that of a siphon; there is a large negative pressure which helps draw the fluid up and the overall flowrate through the rotor is enhanced relative to what could normally be achieved. In fact, because of this siphoning, the total liquid volume in the rotor for this high flow rate case is actually slightly less than for the 600 ml/min case.

While this behavior has not been directly observed experimentally (e.g., with a transparent upper weir cap), its effects certainly have been. It was noted by Leonard et al. (5) that there were unexplained effects that caused an elevation in the zero-point flow rate for large upper weir radii for which the zero-point flow rate was in excess of 2000 ml/min. Other researchers have also noted unpredictably high flow rate behavior including a variable zero-point accompanied by oscillatory outlet flow (6). This oscillatory behavior is not unexpected based on the simulation predictions outlined here. While the "water ring" predicted here was apparently stable, it could be imagined that the corresponding seal ring that forms in the real system could easily be disrupted by surface imperfections and/or could exhibit a cyclic formation–growth–breakdown type behavior over certain flow rate ranges. In general, this behavior of the flow above the upper weir and the corresponding elevation of the zero-point can be considered deleterious as it restricts the ability to select appropriate weir dimensions that have predictable and consistent operation over the entire range of desired flow rates.

Regarding the creation of this water ring, the droplet linking that was seen for the 600 ml/min flow rate case may lend some insight into the general formation mechanism. Several potential methods for ameliorating this behavior (by design) are also readily apparent. Two ideas are shown in Fig. 10. One might give the outlet channels a slight reversed slant in order to increase "pumping" of liquid out of this region (Fig. 10(b)). Similarly, the weir cap and outlet channel could be modified as shown in Fig. 10(c) such that the water ring is disrupted because the outer edge is no longer a continuous circle. More substantial changes could also be

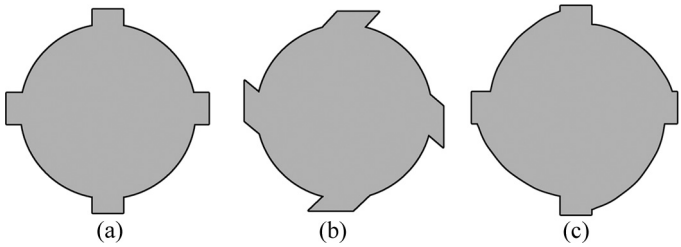

Figure 10. Sketches of a couple possible modifications to the cross-sectional profile of the upper weir cap. The current standard configuration is shown in (a).

envisioned such as adding vanes in this upper section to help propel the fluid out of this region. The effectiveness of any of these potential modifications could easily be explored through similar CFD simulations.

Prediction of Zero Point Flow Rate

The single phase flow rate at which the separation zone fills and all of the flow can no longer go over the upper weir is called the "zero-point" flow rate, and is a useful quantity for rotor flow characterization. For example, the zero-point flow rate is used in practice to verify fabrication consistency of a set of rotors with the same specifications, such as might be used in a multi-stage bank of contactors.

By employing hydrostatic arguments and flow correlations using analogy to the gravity separation trough as sketched in Fig. 2, it is possible to obtain an accurate prediction of the zero-point flow rate for a given rotor geometry. However, as was shown in the previous section, there are regions of flow where the assumptions required for this type of analysis are not valid. Flow simulations of the type outlined here are a useful secondary tool for determining the zero-point flow rate and explaining "off-normal" experimental observations.

Experimentally, the zero-point is identified by the flow rate at which flow begins to come out of the light phase exit. This condition is difficult to converge on either with the hydrostatic rotor models or with the present simulations. For the hydrostatic models, convergence to a non-zero value of flow from the light phase exit requires tedious manual iteration. Similarly for CFD simulations, the pre-defined endpoint of a non-zero outlet flow is difficult to determine.

Thus, it was chosen for the CFD simulation-based prediction method developed here to define the "zero-point" of the simulation as the flow rate at which the air/water interface is positioned exactly at the edge of the lower weir (i.e. $r_{interface} = r_{w,lower}$). While this introduces some

ambiguity in direct comparison with experiment, it also eliminates the effects of surface adhesion and surface tension on the weir edge which, though physically included in the modeling, would make identification and definite demarcation of the zero-point difficult were a steady, non-zero value for flow over the lower weir desired. The primary purpose of these simulations for prediction of the zero-point was to understand the effects of the weir cap and "water seal" described above, and such ambiguity relative to experiment was deemed of secondary importance. Consequently, the zero-point flow rate measured experimentally would be somewhat higher than the effective zero-point determined here by simulation. This is further compounded by the sharp versus beveled weir effect that was noted previously which would also likely tend to increase the predicted zero-point flow rate by increasing the effective pressure drop of the flow over the sharp-edged weir relative to the beveled one.

Different meshing was employed for the zero-point flow rate simulations in order to decrease the total number of cells and speed up the overall calculation. The zero-point flow rate was calculated for two different upper weir radii, 1.15 cm and 1.08 cm. Simulations were performed for each of these weir radii for a geometry employing the standard weir cap and one with a modified "vented" weir cap to be described below.

Calculation Method

Prediction of the zero-point flow rate was done through a code module (written by Wardle) and linked to the CFD simulations to couple the inlet flow rate with the overall mass balance and the position of the interface (air/water) relative to the lower weir. The general outline of the scheme for determining the zero-point flow rate is as follows:

1. For the current flow rate setting, perform a specified number of time steps (iterations).
2. Calculate overall mass balance ($\sum \dot{m}_{out} - \sum \dot{m}_{in}$) and determine if system is at steady-state.
3. If system is at steady-state, change inlet flow rate proportional to the deviation of the current average position of the air/water interface $\overline{r_{int}}$ from the setpoint ($\overline{r_{int}} = r_{w,lower}$). Return to step 1.
4. If system is not yet at steady-state for the current flow rate setting, do not change flow rate. Return to step 1.
5. Stop the simulation when the setpoint is reached ($\overline{r_{int}} - r_{w,lower} \approx 0$).

Steady-state in step 2 above was defined as a deviation of less than 2.5% in the overall mass balance averaged over 250 time steps

(approximately 75 ms). It was found that this was a sufficient number of time steps to achieve a steady value in the overall mass balance. Once it was determined that steady-state was achieved at the current flow rate setting, the flow rate was changed proportional to the setpoint of the defined "zero-point" (the gas-liquid interface position, $\overline{r_{int}}$, at the lower weir radius, $r_{w,lower}$) according to:

$$\dot{m}_{in,new} = \alpha \cdot \dot{m}_{in,old}\left(1.0 + \frac{\overline{r_{int}} - r_{w,lower}}{r_{w,lower}}\right) \tag{2}$$

where $\dot{m}_{in}$ is the inlet mass flow rate and α is an under-relaxation factor that was set to 0.25 to ensure smooth convergence to the zero-point and avoid overshoot. The air/water interface position $\overline{r_{int}}$ was defined as the average radial position of the interface (time- and spatially-averaged over the same 250 time steps) in the region beginning at the top of the light phase weir and extending 5 mm below the weir. The interface is defined as the surface of constant water volume fraction $\phi = 0.5$. As an example, from Eq. 2 we see that if the radial position of the air/water interface $\overline{r_{int}}$ is greater than the lower weir radius $r_{w,lower}$ the flow rate is increased correspondingly resulting in an increase in the fluid volume in the rotor and a shift in the interface position moving it closer to the light phase weir radius (i.e., a decrease in r_{int}).

While several potential weir cap modifications were presented in Fig. 10, a simple modification to the weir cap was chosen that did not significantly alter the general flow behavior but still allowed for communication of pressure between the air space above the weir and the outside pressure. This was done by introducing a small hole, or vent, in the weir cap near the rotor shaft. A so-modified "vented" weir cap was constructed and a snapshot of the underside of the cap is shown in Fig. 11. Since the simulation geometry was a quarter section, it actually had four of these semi-circular vents. The modified model geometry can be seen in the image of the flow for the vented geometry given in the following section (Fig. 13). The effect of the closed upper weir cap was thus explored both through experimental comparison of the measured zero-points and corresponding simulations for the two different caps.

Zero-Point Predictions

Simulations were performed to determine the zero-point flow rate for each of the four cases outlined above (1.08 cm weir Standard and Vented, 1.15 cm weir Standard and Vented). The resulting predictions are presented in Table 3 along with the experimentally observed values for

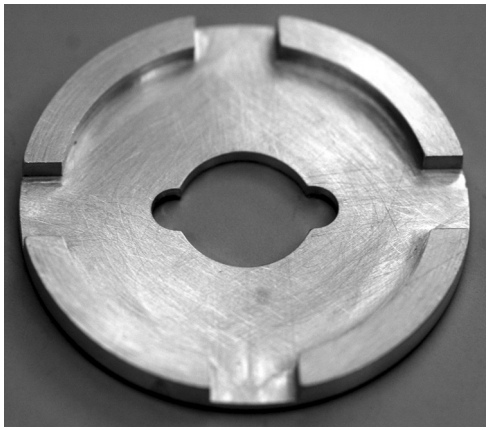

Figure 11. Image of the underside of the 'vented' upper weir cap.

comparison. A difference between the predictions and experiments is anticipated because of the difference in the definition of the zero-point between the two and perhaps also due to the beveled inner edge on the upper weirs used in the experiment. This level may create a lower pressure drop in this region relative to a sharp-edged weir and thus tend to result in a higher zero-point flow rate. Experimental measurement of the zero-point flow rate was made using the two different weirs for which simulations were performed (1.08 cm and 1.15 cm) with both the standard "closed" upper weir cap and the modified "vented" one. Additionally, experimental measurements using a larger weir (1.175 cm) were also made to further explore the differences between the standard and vented caps.

For the smallest weir ($r_{w,upper} = 1.08$ cm), there was no difference in the predicted zero-point value from the simulations. Interestingly, there was a slight elevation ($\sim$15%) in the experimentally measured zero-point for the standard cap relative to the vented one. For this pair of experiments, the inlet flow rate was gradually increased and the zero-point flow rate was defined as the average value of the first total flow rate setting at which flow from the light phase exit was observed and the last setting at which no flow was observed. Plots of the measured flow rate out of the light phase exit versus the total inlet flow rate for the two weir caps are given in Fig. 12. It is not certain that the observed difference is significant. As can be seen by comparing the value for the standard cap measured in this current work and the one reported previously by Leonard et al. (5), there is some variability in measurement of the zero-point. The simulations did in fact predict a slight difference in the pressure above the upper weir for the two cases. The pressure above

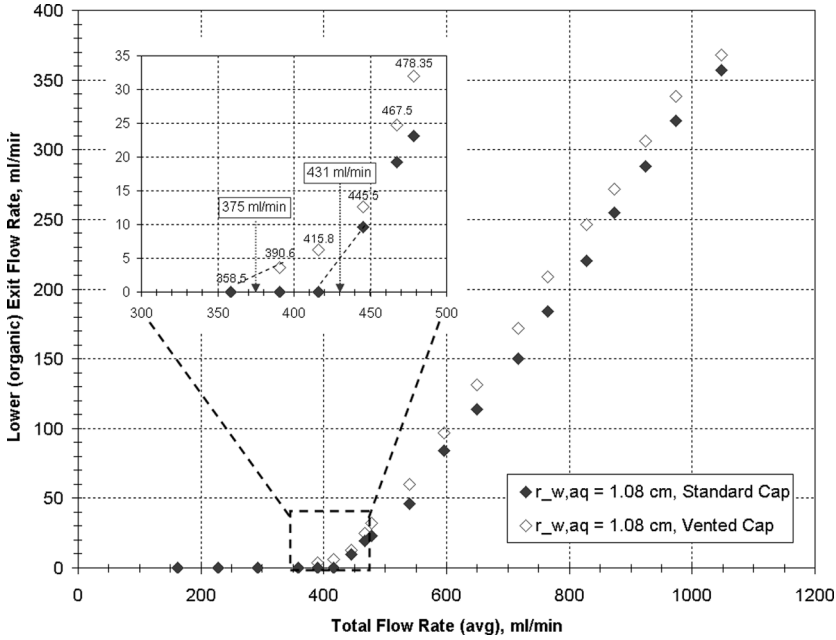

Figure 12. Plot of zero-point flow rate measurements for the 1.08 cm upper weir using the standard (closed symbols) and vented (open symbols) weir caps.

the upper weir was approximately −40 Pa for the standard case and only −20 Pa for the vented case. This slight excess negative pressure in the standard cap case may be the source of the measured zero-point elevation that was seen even for this relatively low flow rate where the exit ports remain fully ''open''.

For the $r_{w,upper} = 1.15$ cm weir size, there is a significant increase in the predicted zero-point flow rate caused by the siphon effect of the ''water seal'' maintained in the standard closed upper weir cap; the prediction for the standard weir cap was 54% higher than for the vented cap. It was verified that for this flow rate (2230 ml/min) the standard cap had a sealing ring of water similar to that shown previously in Fig. 9 for 1600 ml/min. The thickness of the water ring did not appear to have changed significantly and was still ~2 mm thick; however, the air pressure above the upper weir was found to be only approximately −675 Pa (compared to −1900 Pa in the 1600 ml/min case). With the introduction of the vent in the upper cap into the simulated rotor geometry, the sealing water ring was observed to immediately break down and the flow above the upper weir quickly returned to a general pattern of droplet flow as shown in Fig. 13. While some droplet linking flow can

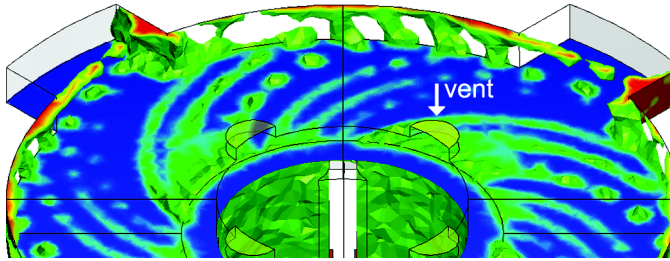

Figure 13. Instantaneous flow of water above the upper weir at the predicted zero-point (1451/ml/min) for the vented cap and the 1.15 cm upper weir (online version contains color reproduction).

be seen around the outer edge of the weir cap, the liquid in this region is still discontinuous and the exit ports remain open. While the general flow pattern seen here is similar to that shown in Fig. 8, the pressure above the upper weir was found to be 0 Pa in this case as compared to approximately −30 Pa for the flow with the standard cap at 600 ml/min. Also, the film thickness at the backside of the exit channels is understandably somewhat greater than seen at the lower flow rate. The experimental measurements show the same trend in zero-point elevation for the closed upper cap relative to the vented one. The zero-point for the vented case is approximately 17% less than the closed cap case. While this difference is not as dramatic as predicted by the simulation, it evidences the same behavior—a negative pressure above the upper weir that elevates the zero-point flow rate for the rotor with the closed upper cap.

For the largest upper weir size tested (1.175 cm), the elevation in the experimentally observed zero-point for the closed cap case relative to the vented one was more substantial (26%). Note that the zero-point reported here for the standard cap case is somewhat less than that reported for the same weir by Leonard et al. (5). The reason for this difference is not clear and may be related to a different delineation of the zero-point between the two studies (e.g., measurable outlet flow versus the first visual observation of flow in the light phase collector ring). It may also be that the difference is due to variability in the formation and stability of the sealing water ring and siphon above the upper weir.

It is clear from these simulations that the restricted flow space above the upper weir due to the weir cap has a significant effect on the zero-point flow rate. These simulations help to explain the zero-point elevation that was observed previously for high flow rates in the CINC V-2 contactor (5). In that study, the principle author also postulated that the degree of air-tightness of the upper weir cap around the rotor shaft may have had some effect on these off-normal zero-point effects; these simulations

indeed predict such behavior. In that study, however, this effect was only observed for weirs greater than 1.15 cm (with zero-points $\gtrsim$ 2500 ml/min). The current simulations have predicted this behavior at flow rates as low as 1600 ml/min; an incremental range of flow rates was not explored in order to determine the specific flow rate at which this behavior first arises. The effect of liquid surface contact and perhaps even surface roughness in the region above the upper weir would likely have an effect on the specific conditions at which this water siphon forms as well as on its overall stability. Note also that Leonard et al. (5) observed that the weirs for this 5 cm contactor had an "apparent" size somewhat greater than the actual size which may be evidence of an additional effect due to the beveled weir edge.

CONCLUSIONS

The flow in the separation zone of the annular centrifugal contactor has been explored through the application of detailed computational flow simulations of the actual geometry of a model rotor of a CINC V-2 centrifugal contactor. It was found that there is indeed a vertical column of air that develops along the axis of the spinning rotor. For moderate flow rates the heavy phase exit ports above the upper weir remain open and there is droplet flow over the weir. At high flow rates, the flow area above the upper weir becomes sealed with water and forms a siphon which increases the amount of flow that can pass over the upper weir. This was observed quantitatively through prediction of the zero-point flow rate for the standard sealed upper weir cap and for one with venting. Similar trends between the two weir caps were also observed experimentally. This research effort has viewed the contactor from the perspective of solvent extraction and has therefore deemed the zero-point elevation an undesirable quality. For operation of the contactor primarily as a dedicated separation device, it might be argued that a higher heavy phase throughput is advantageous. Even so, it can generally be concluded that a predictable throughput is preferable regardless of the application of the unit.

These simulations provide a detailed view of the flow structures within the rotor of the centrifugal contactor. In particular, specific details of the flow above the upper weir have helped to explain previously observed behaviors for this design of contactor rotors. As this commercial contactor design has been in general favorably evaluated for solvent extraction use by a number of studies (5,9,11,17), the research presented here provides a tool for evaluating the design as well as a method for enabling greater general understanding of the flow and hydraulic operation of the separation zone of the annular centrifugal contactor.

ACKNOWLEDGEMENTS

The authors would like to thank Mark Anderson for assistance with the experimental setup for the measurements. Thanks also to Ralph Leonard of Argonne National Laboratory for many helpful discussions and for contributing his vast contactor experience to provide encouragement and support for the simulation results. This research was performed under appointment to the U.S. Department of Energy Nuclear Engineering and Health Physics Fellowship Program sponsored by the U.S. Department of Energy's Office of Nuclear Energy, Science, and Technology. This work was partially supported by the National Center for Supercomputing Applications under TG-ECS070009 and utilized the Tungsten Cluster.

REFERENCES

1. Vandegrift, G.F.; Regalbuto, M.C.; Aase, S.; Bakel, A.; Battisti, T.J.; Bowers, D.; Byrnes, J.P.; Clark, M.A.; Emery, J.W.; Falkenberg, J.R.; Gelis, A.V.; Pereira, C.; Hafenrichter, L.; Tsai, Y.; Quigley, K.; Vander Pol, M.H. (2004) Designing and demonstration of the UREX + process using spent nuclear fuel. In The International Conference on Advances for Future Nuclear Fuel Cycles, ATALANTE, Nimes, France, June 21–24, 2004.
2. Bernstein, G.; Grosvenor, D.; Lenc, J.; Levitz, N. (1973) Development and performance of a high-speed annular centrifugal contactor. Technical Report ANL-7969, Argonne National Laboratory.
3. Wardle, K.E. (2008) *Computational and Experimental Analysis of the Flow in an Annular Centrifugal Contactor*; Ph.D. dissertation, University of Wisconsin-Madison.
4. Leonard, R.; Pelto, R.; Ziegler, A.; Bernstein, G. (1980) Flow over circular weirs in a centrifugal field. *Can. J. Chem. Eng.*, *58*: 531.
5. Leonard, R.; Regalbuto, M.; Aase, S.; Arafat, H.; Falkenberg, J. (2002) Hydraulic performance of a 5-cm contactor for caustic-side solvent extraction. Technical Report ANL-02/18, Argonne National Laboratory.
6. Leonard, R.A. (March 2008) private communication.
7. Wardle, K.E.; Allen, T.R.; Anderson, M.H.; Swaney, R.E. (2008) Free surface flow in the mixing zone of an annular centrifugal contactor. *AIChE J*, *54*: 74.
8. Wardle, K.E.; Allen, T.R.; Anderson, M.H.; Swaney, R.E. (2009) Analysis of the effect of mixing vane geometry on the flow in an annular centrifugal contactor. *AIChE J.*, (in press).
9. Birdwell, J.F.; Anderson, K.K. (2001) Evaluation of 5-cm centrifugal contactor hydraulic and mass transfer performance for caustic-side solvent extraction of cesium. Technical Report ORNL/TM-2001/137, Oak Ridge National Laboratory.
10. Birdwell, J.F.; Anderson, K.K. (2002) Evaluation of mass transfer performance for caustic-side solvent extraction of cesium in a conventional 5-cm

centrifugal contactor. Technical Report ORNL/TM-2001/278, Oak Ridge National Laboratory.
11. Law, J.; Tillotson, R.; Todd, T. (2002) Evaluation of the hydraulic performance and mass transfer efficiency of the CSSX process with the optimized solvent in a single stage of 5.5-cm diameter centrifugal contactor. Technical Report INEEL/EXT-02-01106, Idaho National Engineering and Environmental Laboratory.
12. Padial-Collins, N.T.; Zhang, D.Z.; Zou, Q.; Ma, X. (2006) Centrifugal contactors: Separation of an aqueous and an organic stream in the rotor zone (LA-UR-05-7800). *Sep. Sci. Technol.*, *41*: 1001.
13. Wardle, K.E.; Allen, T.R.; Anderson, M.H.; Swaney, R.E. (2008) Experimental study of the hydraulic operation of an annular centrifugal contactor with various mixing vane configurations. (submitted for publication).
14. Brackbill, J.; Kothe, D.; Zemach, C. (1992) A continuum method for modeling surface tension. *J. Comput. Phys.*, *100*: 335.
15. Fluent Inc.. (2006) Fluent 6.3 User's Guide.
16. Sheldon, B.V.; Flim, W.D.; Mendoza, G.; Macaluso, L.L. Method of making an easily disassembled rotor assembly for a centrifugal separator. US Patent 6,363,611 B1, April 2, 2002.
17. Law, J.; Meikrantz, D.; Garn, T.; Mann, N.; Herbst, S.; Todd, T. (2006) The testing of commercially available engineering- and plant-scale annular centrifugal contactors for the processing of spent nuclear fuel. Technical Report INL/CON-06-11498, Idaho National Laboratory.